ADVANCED FUNCTIONAL MATERIALS

Supporting Information

for *Adv. Funct. Mater.*, DOI: 10.1002/adfm.202000239

The Vibration Behavior of Sub-Micrometer Gas Vesicles in Response to Acoustic Excitation Determined via Laser Doppler Vibrometry

*Shuai Zhang, An Huang, Avinoam Bar-Zion, Jiaying Wang, Oscar Vazquez Mena, Mikhail G. Shapiro, and James Friend**

Supporting Information Available

Agar phantom scan

Gas vesicles have strong ultrasound contrast due to the gas encapsulated within them, as indicated with an 18 MHz transducer (L22–14v, Verasonics, Kirkland, WA USA) in Fig. S1(a). Moreover, some gas vesicle variants, such as stripped Ana GVs as the focus of this study, have nonlinear contrast (Fig. S1b). This facilitates the use of amplitude modulation schemes to produce a highly specific map of GV distribution within the imaging plane. If needed, high hydrostatic or ultrasonic pressure can collapse GVs, "erasing" their signals, as performed here with the 18 MHz transducer at 2.09 MPa to produce Fig S1(c).

FTIR Results

The gold substrate is not active in the infrared range of 1400–2400 cm^{-1}, so no reduction in the transmission appears over this range in Suppl. Fig. S2(a). After biotin is bound to the gold with CA and ME as the middle layer, significant reductions in transmission are found as seen in Fig. S2(b). The most obvious peak is at 1680 cm^{-1}, which corresponds to the amide I vibration mode together with the C=O stretch of biotin. This result tells us that the gold substrate is bonded with NHS-biotin.

Exploring the possibility that the GVs are simple bubbles

The importance of the elastic membrane used in the main portion of the text in the modified Rayleigh-Plesset equation is best illustrated by computing the resonance frequencies of a representative bubble that *lacks* this membrane. Using the classic Rayleigh-Laplace equation,

$$f^2 = \frac{\sigma}{R^3}\frac{(j-1)(j+1)(j+2)}{(j+1)\rho^+ + j\rho^-}, \tag{4}$$

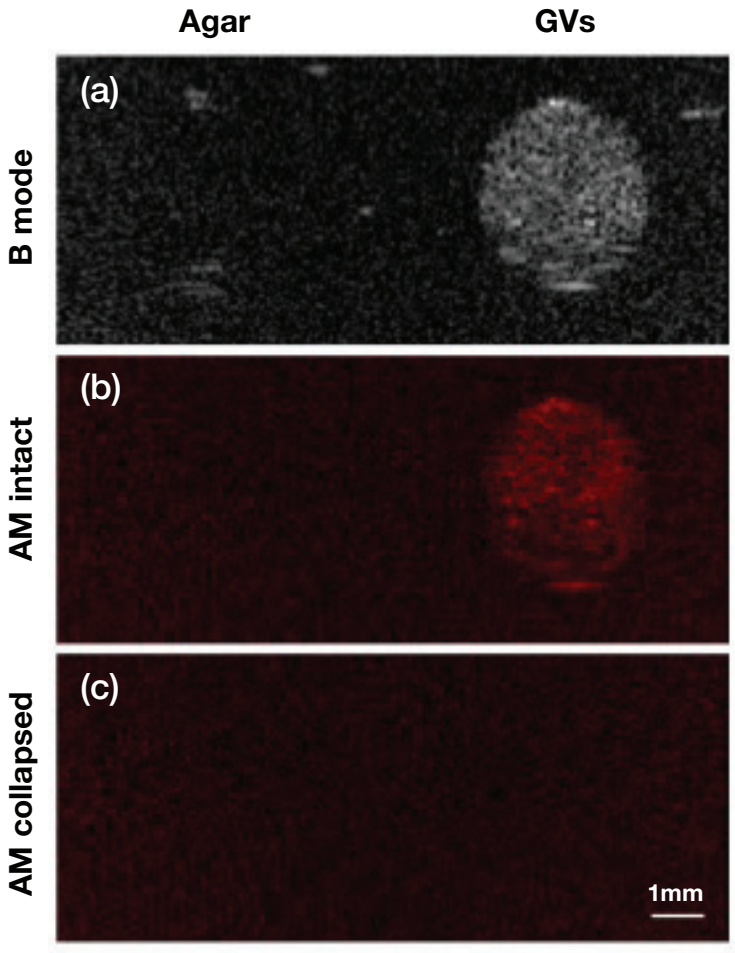

Figure S1: Linear and non-linear ultrasound contrast images of stripped Ana GVs. (a) The linear contrast of GVs can be detected using an anatomic B-mode ultrasound scan at 18 MHz. The result of the scan for an agar-filled well is provided for comparison on the left. (b) The non-linear contrast of stripped Ana GVs can be observed using the amplitude modulation pulse sequence. (c) If necessary, the GVs can be "erased" via apparent collapse using high pressure; in this case 2.09 MPa ultrasound from a commercial transducer.

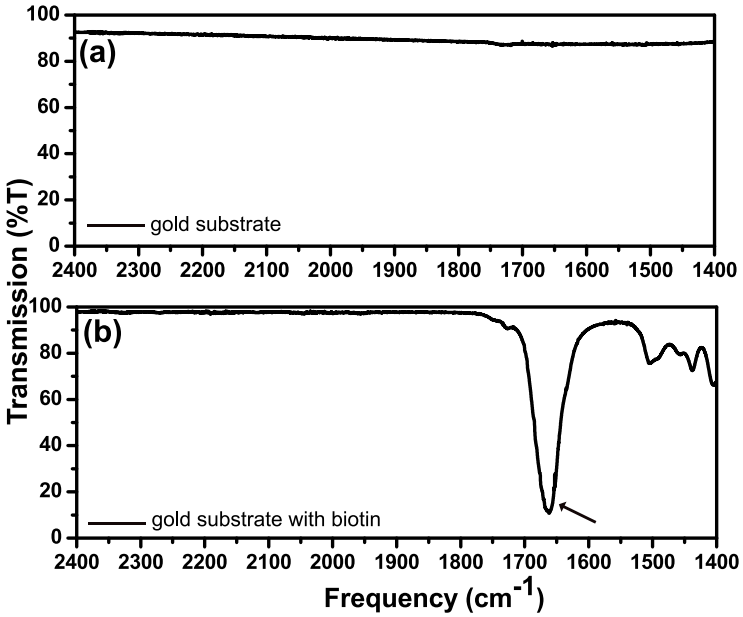

Figure S2: FTIR results indicate that compared to the (a) response of a pure gold substrate prior to before any treatment, (b) biotin produces significant transmission changes after binding it to the gold substrate using CA and ME. The arrow in (b) indicates a characteristic peak at 1680 cm^{-1} associated with the NHS-biotin bond.

with the dimensions and properties chosen to match the GV in a manner similar to the coated bubble calculations, where σ is the protein-air surface tension (0.2 mN/m^2), R is the radius of the bubbles, j is the mode number ($j > 1$), ρ^+ is the density inside the bubbles, and ρ^- is the density outside the bubbles.[42] The fundamental and first harmonic resonance frequencies predicted by this equation are 190 MHz and 301 MHz, substantially less than the corresponding observed experimental results of 1.02 GHz and 1.7 GHz.

Exploring the possibility that the GVs are solid particles

It could be that the GVs are in fact solid nano-sized particles. We consider the resonance frequencies that solid GVs would produce using a classic equation from Lamb.[43] The equation defines the fundamental resonance frequency of a solid sphere f_{solid} through the relationship $\frac{f_{\text{solid}}^2 \rho}{Y} R^2/(4\pi^3) \approx 1.8$. Treating the allantoid shape as approaximately spheriod, and equating the volume, the radius of an equivalent sphere is $R = 1.3 \times 10^{-7}$ m, and $\rho \sim 10^3$ kg/m^3 and

$Y \sim 3$ GPa[13] are the density and rigidity, the lowest possible resonance frequency is on the order of 10^{11} Hz. The high Young's modulus comes from the protein layer. The resonance frequency from this calculation shows that it is two orders of magnitude greater than our observations, suggesting that GVs are not solid particles.

Mode shapes of surface-bound and free GVs of different lengths

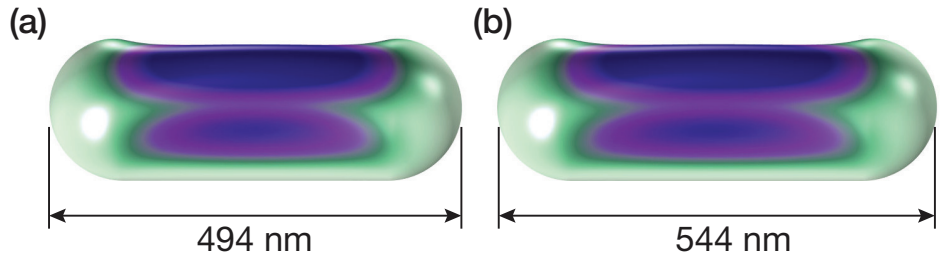

Figure S3: The computed mode shapes of a surface-bound GV, with one-eighth of the cylindrical portion of the GV nearest the bottom fixed in place, representing binding to a surface. The length of the GV is different (a) 494 nm and (b) 544 nm with resonance frequency at 1.092 GHz and 1.088 GHz, respectively, within 4.3% of the experimentally measured fundamental resonance frequency at 1.047 GHz.

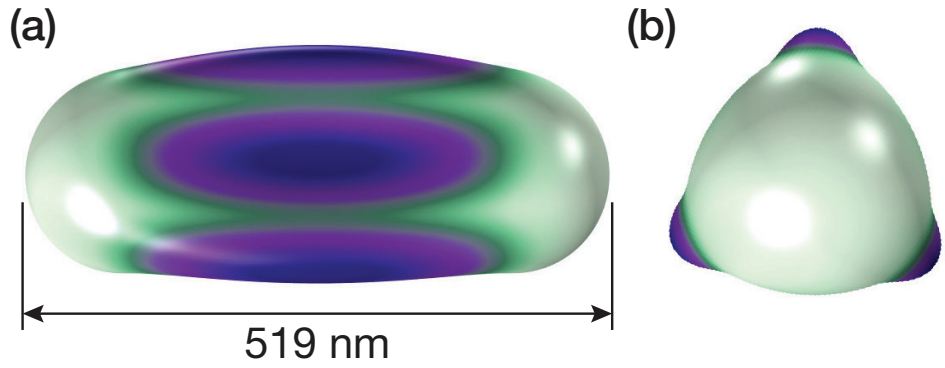

Figure S4: A GV completely free to move produces a computed fundamental resonance frequency of 0.992 GHz, remarkably only 6.8% less than the experimentally measured fundamental resonance frequency of 1.047 GHz for bound and agglomerated GVs.

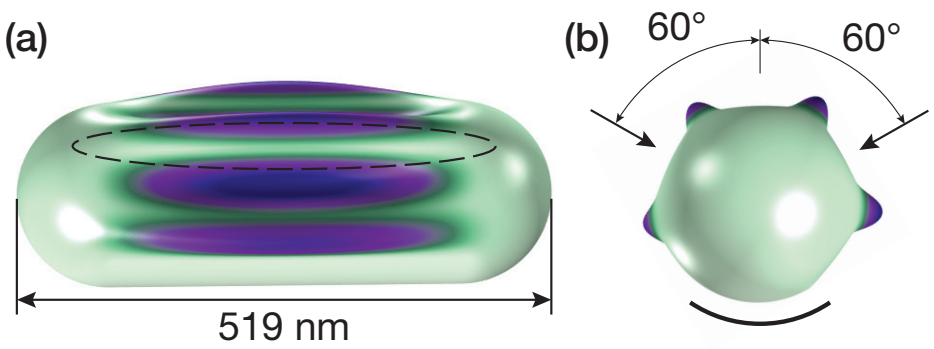

Figure S5: The computed mode shapes of a surface-bound GV; with it bound with other GVs at 60° from the vertical via symmetry boundary conditions. The boundary conditions are applied along lines defined upon the GV's cylindrical portion, one shown and one hidden upon the back side of this GV; and one-eighth of the cylindrical portion of the GV nearest the bottom fixed in place as indicated with the heavy curved line in the end view. Each symmetry-bound agglomeration line lies 45° from the vertical and is along the cylindrical portion of the allantoid shape. The fundamental resonance frequency produced by this object is 1.06 GHz, 1.2% above the 1.047 GHz resonance found for the GVs in our experiments.

Resonance response of GVs at 300 MHz depends upon GV agglomerate size

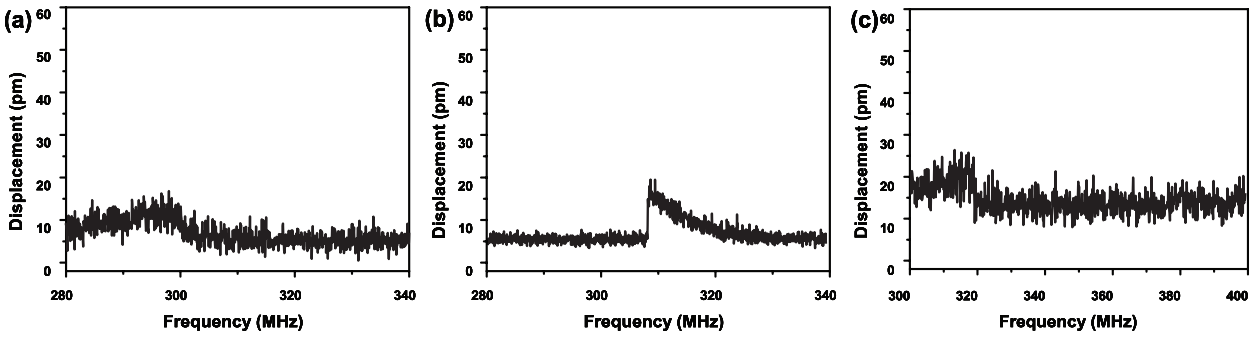

Figure S6: Resonances observed via the LDV at (a) close to 295 MHz, (b) close to 310 MHz, and (c) close to 310 MHz around appear to arise from the vibration of GV agglomerations of around 615 nm in size (*see* main text for details).

The measured transducer output vibration amplitude and pressure as dependent upon the input power

Table S1: The measured amplitude of vibration upon the transducer and the calculated acoustic pressure in the fluid adjacent the transducer, depending upon the power input into our transducer

Input power (W)	Displacement (nm)	Calculated acoustic pressure (kPa)
1	0.700	89
2	1.04	132
3	1.4	178
4	1.67	212
5	1.9	242
6	2.6	330
7	2.8	356